

Real-Time History of the Cosmological Electroweak Phase Transition

H. Kurki-Suonio^{a,*} and M. Laine^{b,†}

^a*Department of Physics, P.O.Box 9, FIN-00014 University of Helsinki, Finland*

^b*Institut für Theoretische Physik, Philosophenweg 16, D-69120 Heidelberg, Germany*
(August 1, 1996)

We study numerically the real-time history of the cosmological electroweak phase transition, as it may take place in the Standard Model or in MSSM for $m_H \lesssim m_W$ according to recent lattice results. We follow the nucleated bubbles from the initial stages of acceleration and rapid growth, through collisions with compression waves resulting in slowing down and reheating to T_c , until the final stages of slow growth and evaporation. We find that collisions with compression waves may make the bubble walls oscillate in the radial direction, and that reheating to T_c takes generically place.

PACS numbers: 98.80.Cq, 47.75.+f, 95.30.Lz

The electroweak phase transition in the early Universe may have had important consequences, like baryogenesis [1]. These depend crucially on the non-equilibrium details of the first-order transition [2]. The general features of the real-time history of first-order cosmological phase transitions have been known for quite a long time [3], and, e.g., the properties of bubble growth soon after the nucleation period have been studied in detail [4–6]. The whole real-time history has also been computed in some approximation [7,8], but a more detailed hydrodynamical investigation has so far been missing. In addition, the relevant parameter values are reliably known only after recent lattice simulations [9]. The purpose of this paper is to present a detailed hydrodynamical study of the complete real-time history of the electroweak phase transition for realistic parameter values.

Before the transition the universe is in the high-temperature ‘symmetric’ phase. As the temperature falls below the critical temperature T_c , the symmetric phase becomes metastable. Bubbles of the ‘broken-symmetry’ phase nucleate at $T_n < T_c$, and grow rapidly. There are two modes of bubble growth at this stage: detonations, which are supersonic, and deflagrations, which are usually subsonic [10,11]. In a deflagration the bubble wall is preceded by a compression wave, whereas in a detonation it is followed by a rarefaction wave. When the bubbles collide, the evolution becomes complicated. We find that the compression waves from neighboring bubbles may cause large-amplitude back-and-forth motion of the bubble wall. Since the baryon number is generated at the wall in a manner sensitive to the wall velocity, these details are important for baryon number production.

The tool used here is a hydrodynamical model where a scalar order parameter ϕ drives the transition [10]. The (non-perturbative) effective potential $V(\phi)$ for the

scalar order parameter is parametrized by the latent heat $\hat{L} \equiv L/T_c^4$, the surface tension $\hat{\sigma} \equiv \sigma/T_c^3$ and the correlation length $\hat{l}_c \equiv l_c T_c$. Non-equilibrium phenomena at the phase transition front are described by a simple friction term, and the corresponding parameter η is deduced from a recent microscopic calculation [6].

The equations of motion follow from energy-momentum conservation and an equation for entropy production [10]. In an expanding universe with metric

$$ds^2 = -dt^2 + R(t)^2(dr^2 + r^2 d\theta^2 + r^2 \sin^2\theta d\phi^2)$$

and in a spherically symmetric case, eqs. (5–7) of [11] become

$$\begin{aligned} \partial_t^2 \phi - \frac{1}{R^2} \frac{1}{r^2} \partial_r (r^2 \partial_r \phi) + 3H \partial_t \phi + \frac{\partial V}{\partial \phi} \\ = -\eta \gamma (\partial_t \phi + v \partial_r \phi), \end{aligned} \quad (1)$$

$$\begin{aligned} \partial_t E + \frac{1}{r^2} \partial_r (r^2 E v) + 3H E \\ + p [\partial_t \gamma + \frac{1}{r^2} \partial_r (r^2 \gamma v) + 3H \gamma] \\ - \frac{\partial V}{\partial \phi} \gamma (\partial_t \phi + v \partial_r \phi) = \eta \gamma^2 (\partial_t \phi + v \partial_r \phi)^2, \end{aligned} \quad (2)$$

$$\begin{aligned} \partial_t Z + \frac{1}{r^2} \partial_r (r^2 Z v) + 5H Z + \frac{1}{R^2} \left[\partial_r p + \frac{\partial V}{\partial \phi} \partial_r \phi \right] \\ = -\frac{1}{R^2} \eta \gamma (\partial_t \phi + v \partial_r \phi) \partial_r \phi. \end{aligned} \quad (3)$$

Here ϵ is the energy density and $w = \epsilon + p$ the enthalpy density, and we have defined $E \equiv \epsilon \gamma$, $Z \equiv w \gamma^2 v$. The velocity v above is the coordinate velocity dr/dt of the fluid, the physical velocity being Rv . The scale factor R changes very little during the period of interest, so the difference is unimportant, but below v will refer to the physical velocity. The main effect of the expansion is the cooling of the universe, where the small change is significant because we are very close to T_c . $H = \dot{R}/R$ is the expansion rate of the universe.

For the thermodynamical properties of the phase transition we use four sets of parameters, suggested by lattice simulations [9]. The main difference with respect to perturbation theory is that the surface tension $\hat{\sigma}$ gets small if the transition is weak. As the first set we take the Standard Model with an unrealistically small Higgs mass $m_H = 51$ GeV (case C):

$$\hat{L} = 0.124, \quad \hat{\sigma} = 0.0023, \quad \hat{l}_c = 8. \quad (4)$$

A second set is $m_H = 68$ GeV in which case the transition is very weak but still of first order (case D):

$$\hat{L} = 0.08, \quad \hat{\sigma} = 0.0002, \quad \hat{l}_c = 10. \quad (5)$$

Both of these cases lead to a transition too weak for baryogenesis. As a third case we consider a stronger transition (case B):

$$\hat{L} = 0.3, \quad \hat{\sigma} = 0.01, \quad \hat{l}_c = 5. \quad (6)$$

This transition corresponds to a tree-level Higgs mass parameter $m_H^* \sim 50$ GeV and is close to being strong enough for baryogenesis [9] (we do not consider the possibilities proposed in [12]). In addition, the values in eq. (6) could be achieved in MSSM for a realistic pole Higgs mass $m_H \lesssim m_W$ [13]. A still stronger transition with $m_H^* \sim 45$ GeV would give $\hat{L} \sim 0.5$, $\hat{\sigma} \sim 0.02$ in MSSM. However, to display more clearly the parameter dependence, we take rather eq. (6) with just a larger surface tension $\hat{\sigma} = 0.02$ (case A).

The dependence of the results on the parameters is roughly the following. The supercooling $1 - \hat{T}_n$ ($\hat{T}_n \equiv T_n/T_c$) and the distances l_n/t_H of the nucleated bubbles ($t_H \equiv H^{-1}$ is the Hubble time, or Hubble length) are proportional to $\hat{\sigma}^{3/2}/\hat{L}$. The velocity of the bubble wall during the rapid growth is proportional to $\hat{\sigma}^{1/2}$. Reheating to T_c takes place if $\hat{L} \gtrsim 8\hat{\sigma}^{3/4}$, and the velocity during the period of slow growth is proportional to $\hat{\sigma}^{3/2}/\hat{L}^2$, provided that this number is small enough. Hence a small $\hat{\sigma}$ indicated by lattice simulations tends to make supercooling and velocities small and reheating likely.

The friction parameter η is determined from the microscopic analysis in [6]. In general, the friction term is non-local and the coefficient η depends on ϕ [14]. However, we do not here study the microscopic structure of the phase transition front and hence η is only used in parametrizing the entropy production. Consequently, we may use a simpler ϕ -independent (but m_H -dependent) η . After determining $\hat{L}, \hat{\sigma}, \hat{l}_c$ and the nucleation temperature \hat{T}_n corresponding to the effective potential used in [6], we search for the value of η producing the same velocity as in Table 1 of [6]. We find that $\eta \sim (0.04 - 0.1)T_c$ for the Higgs masses studied. For completeness we also inspect more general values of η below.

For our four parameter sets A–D, we determine \hat{T}_n and the distances l_n/t_H between the nucleated bubbles [15] with the following simple procedure, giving better accuracy than the classical calculation. The parameters $\hat{L}, \hat{\sigma}, \hat{l}_c$ fix uniquely a quartic potential $V(\phi)$, and for this potential the nucleation action is known analytically with good accuracy [17]. We then solve for \hat{T}_n and l_n/t_H numerically from eqs. (4.5), (4.8) in [5]. By comparing with nucleation calculations for more complicated functional forms of $V(\phi)$, we have found that \hat{l}_c should be interpreted as the correlation length in the broken phase.

case	\hat{T}_n	r_n/t_H	η/T_c	v_{wall}	\hat{r}_{eq}	v_{slow}	$\Delta t/t_H$
A0	0.994938	2.59×10^{-5}	0.003	0.959			2.7×10^{-5}
A1			0.01	0.506			6.7×10^{-5}
A2			0.03	0.490			6.0×10^{-5}
A3			0.10	0.402			7.0×10^{-5}
B1	0.998295	8.73×10^{-6}	0.01	0.406	0.936	0.00149	3.7×10^{-4}
B2			0.03	0.379			
B3			0.10	0.281			
C1	0.999552	2.35×10^{-6}	0.01	0.335	0.796	0.00109	4.4×10^{-4}
C2			0.03	0.288			
C3			0.10	0.170			
D0	0.9999828	9.54×10^{-8}	0.001	0.089	0.311	0.00012	5.6×10^{-4}
D1			0.01	0.084			
D3			0.10	0.046			

TABLE I. The properties of the transition. In case A there is no stage of slow growth, hence no $\hat{r}_{\text{eq}}, v_{\text{slow}}$ are given.

After the nucleation the bubbles start to grow. We have studied the bubble growth with a spherically symmetric hydrodynamical code, which solves eqs. (1–3). We present results for 13 different sets of parameter values (cases A–D with different values of η), see Table I.

The initial stages of bubble growth are not affected by the expansion of the universe or the existence of neighboring bubbles. The bubble wall accelerates and reaches a stationary velocity v_{wall} . The velocity depends on the friction at the wall, parametrized by η . If the supercooling is relatively large, v_{wall} covers most of the range from 0 to 1 as η is varied, and the configuration goes through the different modes described in [10]. For small supercooling, only deflagrations are possible and there is a maximum wall velocity v_{max} [18]. We plot $v_{\text{wall}}(\eta)$ in Fig. 1. Thus in case D the bubble will be a slowly growing deflagration bubble. In cases B and C the bubble has to be a deflagration, but velocities closer to the speed of sound could be achieved. In case A detonations are possible. Case D takes longer to compute, so we show v_{wall} for 3 values of η only.

After the period of stationary growth, the bubbles collide with the compression waves from other bubbles. Our grid length corresponds to $r_n \equiv l_n/2$, and we use reflective boundary conditions at the (spherical) outer edge to represent collisions with the neighboring bubbles. This is an unrealistic geometry, since it makes the collision simultaneous at all points of the bubble wall, preserving the spherical symmetry. Since the nucleation process places the bubbles randomly, in reality every bubble has a different collision geometry. The results presented here give a qualitative idea of the real events, although the aspherical features and transverse motions are missing.

The bubble radius $\hat{r} \equiv r/r_n$ as a function of time for 11 of the 13 cases is shown in Fig. 2. A fraction $f_V = \hat{r}^3$ of the volume is in the broken phase (bubble) and the transition is completed when $\hat{r} = 1$. The microscopic (bubble nucleation radius) and the macroscopic (distance between bubbles) scales in the problem differ by some 9 orders of magnitude. For practical reasons we have set the scales closer to each other on the computer. There-

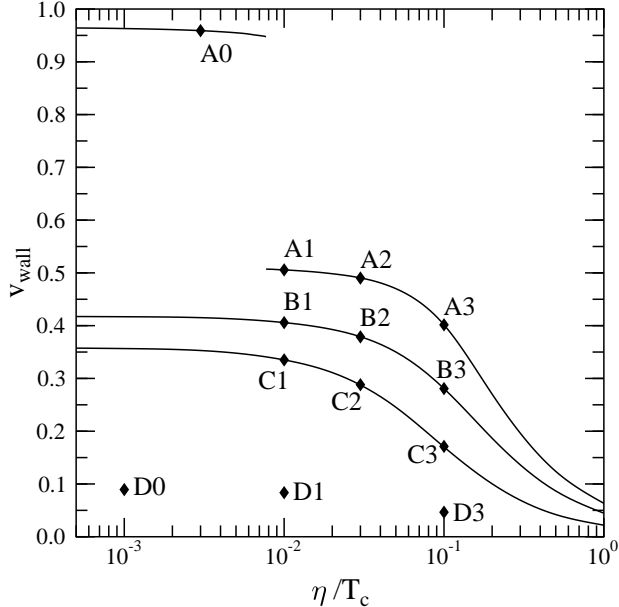


FIG. 1. The wall velocity as a function of η . In case A the wall is a detonation front for $\eta \lesssim 0.0077T_c$. Otherwise the wall is a deflagration front. The black diamonds correspond to the 13 runs discussed in the text.

fore the duration of the initial acceleration stage appears greatly magnified in the figure.

We discuss the fastest-growing bubbles first. In case A0 the bubble wall is a detonation front. No information is transmitted ahead of a detonation, and therefore the wall propagates undisturbed until it collides with the neighboring bubble wall. The phase transition is completed and all the resulting fluid motion takes place in the broken phase.

In all the other cases the bubble wall is a deflagration front, preceded by a compression wave in the symmetric phase. The bubble wall slows down as it meets the compression wave from the neighboring bubble. In most cases studied the compression wave is strong enough to stop the wall and push it back, compressing the bubble. As the compression waves move back and forth between the bubbles, the bubble volume oscillates. In a realistic geometry the bubble is deformed as different parts of the bubble wall move with different velocities. The typical amplitude of the motion should, however, be the same as obtained here. Part of the compression wave is transmitted through the wall into the broken phase, causing partial superheating. In some cases a region inside the bubble may be heated so much that the broken phase cannot exist at this temperature, and a droplet of the symmetric phase is temporarily formed.

Further history of the bubble depends on the magnitude of the latent heat relative to the degree of supercooling. If the latent heat is large enough to reheat the universe back to the critical temperature, both phases can coexist at T_c . The initial volume fraction

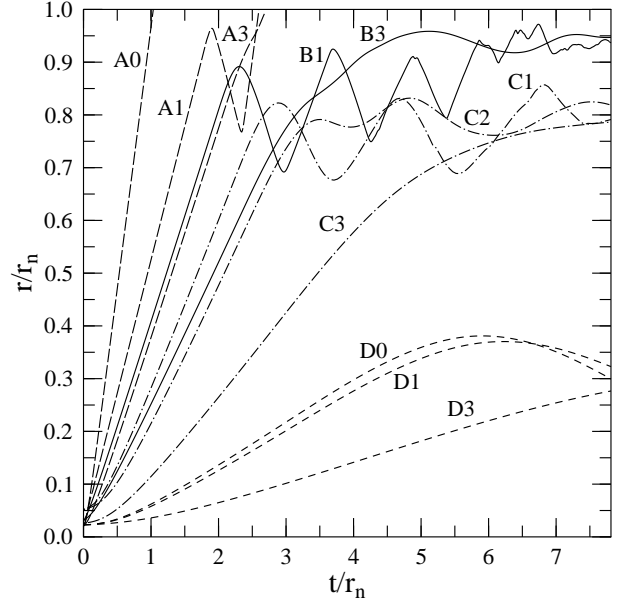


FIG. 2. The bubble radius as a function of time. For clarity the cases A2 and B2 are omitted.

of the broken phase at equilibrium (ignoring the expansion of the universe since bubble nucleation) is then $f_V \equiv \hat{r}_{\text{eq}}^3 = \epsilon_c(1 - \hat{T}_n^4)/L$, where ϵ_c is the energy density of the symmetric phase at T_c . The bubble radius oscillates around \hat{r}_{eq} . The initial amplitude depends on v_{wall} , as deflagrations close to the speed of sound are preceded by strong compression waves which cause large oscillations. A smaller \hat{r}_{eq} also leads to larger oscillations as the compression waves travel longer between the bubbles. The oscillation amplitude decreases with time and the bubble settles to a long period of slow growth.

In case A the nucleation temperature is so low that the universe does not reheat to T_c . The transition is completed after at most one oscillation. The duration of the phase transition Δt is given essentially by the bubble separation and the wall velocity, $\Delta t = r_n/v_{\text{wall}}$. In case A1 the wall changes nature from a deflagration to a detonation after the collision.

In cases B, C, and D, the universe reheats to T_c and the bubble radius oscillates around the equilibrium value \hat{r}_{eq} , given in Table I.

The period of slow growth is paced by the expansion of the universe, which slowly makes space for the released latent heat. This takes a much longer time than the preceding stages, see Fig. 3. To first order in L/ϵ_c , the duration of the phase transition is $\Delta t/t_H = L(1 - \hat{r}_{\text{eq}}^3)/(4\epsilon_c)$, assuming that in the symmetric phase $p \propto T^4$. The wall velocity v_{slow} during the slow growth is geometry dependent, but for the spherical bubble geometry we can estimate it by $v_{\text{slow}} \sim (1 - \hat{r}_{\text{eq}})(r_n/\Delta t)$. The values of $\Delta t/t_H$ and v_{slow} are displayed in Table I. For case D v_{slow} is much less than for the other cases, because the bubbles are much closer to each other.

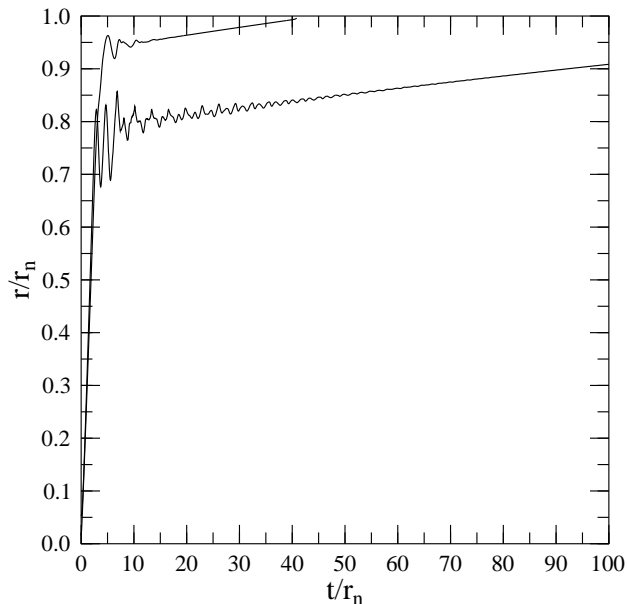


FIG. 3. The bubble history showing the stages of fast and slow growth. The upper line is case B3 and the lower one C1.

At some point during the slow growth the remaining regions in the symmetric phase pull themselves to spherical droplets, resulting in a geometry inverse to the one used above. We have done runs with an inverted geometry, i.e., the shrinking symmetric phase at the center surrounded by the broken phase, starting at a static equilibrium situation at $T \sim T_c$. The droplet evolves first towards the weak deflagration similarity solution described in [19] and the end stages are as found in [11].

The phenomena discussed might have physical significance, e.g., for baryon number generation. Indeed, the velocity dependence of baryon number production may be such that the slowing down of v_{wall} through collisions with compression waves, and the resulting oscillations, have a favourable effect on the baryon number produced [8,2]. It should be noted, however, that for stronger transitions ($D \rightarrow B$) where the baryon number is not washed out afterwards, the fraction of space where the transition proceeds through slow growth is smaller.

Finally, let us note that there remain some important open questions concerning the real-time history. In particular, while the bubble wall appears to be stable during the period of fast growth [20], the period of slow growth is different in character and the stability properties remain open. A related problem is the appearance of turbulence, which might affect, e.g., magnetic fields [21].

We thank J. Ignatius, K. Kajantie, G. D. Moore and M. Shaposhnikov for discussions and the Center for Scientific Computing (Finland) for computational resources. M.L was partially supported by the University of Helsinki.

* Email: hkurkisu@pcu.helsinki.fi

† Email: m.laine@thphys.uni-heidelberg.de

- [1] V. A. Kuzmin, V. A. Rubakov, and M. E. Shaposhnikov, Phys. Lett. B **155**, 36 (1985); M. E. Shaposhnikov, Nucl. Phys. B **287**, 757 (1987).
- [2] V. A. Rubakov and M. E. Shaposhnikov, Usp. Fiz. Nauk **166**, 493 (1996) [hep-ph/9603208].
- [3] P. J. Steinhardt, Phys. Rev. D **25**, 2074 (1982); A. D. Linde, Nucl. Phys. B **216**, 421 (1983), **223**, 544(E) (1983); E. Witten, Phys. Rev. D **30**, 272 (1984); M. Gyulassy, K. Kajantie, H. Kurki-Suonio, and L. McLerran, Nucl. Phys. B **237**, 477 (1984); K. Kajantie and H. Kurki-Suonio, Phys. Rev. D **34**, 1719 (1986).
- [4] M. Dine, R. G. Leigh, P. Huet, A. D. Linde, and D. Linde, Phys. Rev. D **46**, 550 (1992); N. Turok, Phys. Rev. Lett. **68**, 1803 (1992); B. H. Liu, L. McLerran, and N. Turok, Phys. Rev. D **46**, 2668 (1992); S. Yu. Khlebnikov, Phys. Rev. D **46**, 3223 (1992); P. Arnold, Phys. Rev. D **48**, 1539 (1993); G. Moore and T. Prokopec, Phys. Rev. Lett. **75**, 777 (1995).
- [5] K. Enqvist, J. Ignatius, K. Kajantie, and K. Rummukainen, Phys. Rev. D **45**, 3415 (1992).
- [6] G. D. Moore and T. Prokopec, Phys. Rev. D **52**, 7182 (1995).
- [7] M. E. Carrington and J. I. Kapusta, Phys. Rev. D **47**, 5304 (1993); D. Bödeker, W. Buchmüller, Z. Fodor, and T. Helbig, Nucl. Phys. B **423**, 171 (1994).
- [8] A. F. Heckler, Phys. Rev. D **51**, 405 (1995).
- [9] K. Kajantie, M. Laine, K. Rummukainen, and M. Shaposhnikov, Nucl. Phys. B **466**, 189 (1996); M. Gürtler, E.-M. Ilgenfritz, J. Kripfganz, H. Perlt, and A. Schiller, hep-lat/9512022; hep-lat/9605042.
- [10] J. Ignatius, K. Kajantie, H. Kurki-Suonio, and M. Laine, Phys. Rev. D **49**, 3854 (1994); H. Kurki-Suonio and M. Laine, Phys. Rev. D **51**, 5431 (1995).
- [11] H. Kurki-Suonio and M. Laine, hep-ph/9512202.
- [12] W. H. Tang and J. Smit, hep-lat/9605016; M. Joyce, hep-ph/9606223.
- [13] M. Carena, M. Quirós, and C. E. M. Wagner, hep-ph/9603420; J. R. Espinosa, hep-ph/9604320; J. M. Cline and K. Kainulainen, hep-ph/9605235; M. Laine, hep-ph/9605283.
- [14] We thank G. D. Moore for pointing out that to leading order $\eta \sim 0.05\phi^2/T_c$ according to [6], independent of m_H .
- [15] ‘Subcritical bubbles’ (e.g. [16]) refer to the breakdown of perturbation theory at large m_H , and are of no concern here since non-perturbative lattice results are used.
- [16] M. Gleiser and A. F. Heckler, Phys. Rev. Lett. **76**, 180 (1996), and references therein.
- [17] J. Ignatius, Phys. Lett. B **309**, 252 (1993).
- [18] H. Kurki-Suonio, Nucl. Phys. B **255**, 231 (1985).
- [19] L. Rezzolla, J. C. Miller, and O. Pantano, Phys. Rev. D **52**, 3202 (1995).
- [20] P. Huet, K. Kajantie, R. G. Leigh, B.-H. Liu, and L. McLerran, Phys. Rev. D **48**, 2477 (1993).
- [21] G. Baym, D. Bödeker, and L. McLerran, Phys. Rev. D **53**, 662 (1996).